ChemTexts (2020) 6:2
https://doi.org/10.1007/s40828-019-0097-0

LECTURE TEXT

The extended Kubelka–Munk theory and its application to spectroscopy

R. Alcaraz de la Osa[1] · I. Iparragirre[1] · D. Ortiz[1] · J. M. Saiz[1]

Received: 15 August 2019 / Accepted: 18 November 2019 / Published online: 9 December 2019

Abstract

The Kubelka–Munk theory is one of the main theories of light flux through homogeneous isotropic media. In this work, we used the extended solution of this theory, applied to a specimen on top of an arbitrary substrate, to obtain the overall spectral reflectance and transmittance. A complete colorimetric study can be derived from these calculations and this is shown by analyzing the effect of the different properties of the system (scattering and absorption coefficients, thickness, particle radius, surrounding medium) on its coordinates on the color space. Along with the analytical solutions to the original two-flux and the more modern four-flux models, we present a computing tool based on a Monte Carlo algorithm, which is very adequate in this context. In it, both the energy and the media are discretized, and the interaction is converted into probability of scattering and absorption. This numerical procedure also introduces new capabilities in the model, since it admits properties such as inhomogeneity in the layers, or more complex light–matter interactions, and offers solutions with temporal resolution, something applicable, for example, to pulses or transient states.

Keywords Kubelka–Munk · Dense media · Beer–Lambert law · Reflectance and transmittance spectroscopy · Colorimetry · Monte Carlo

Introduction

The propagation of light in scattering/absorbing media is a topic that is addressed very often, with different approaches and with very diverse interests. Historically it is important to mention the bidirectional model of radiation propagation proposed by Schuster [1] in the field of astrophysics, a precursor study of the famous Kubelka–Munk model [2], developed for paints and applied in areas such as paper [3, 4], plastics [5], textiles [6], or the food industry [7], to mention just a few examples. In all these applications the propagation of light, even being a volume problem, is a key aspect in the behavior of surfaces. This is because the surface reflectance must be understood as a process that is the sum of two: one by which part of the light is returned at the interface, and another by which the light enters the medium, travels inside, and exits the medium through the same surface. While the first one is obtained by application of the boundary conditions on the incident field and depends only on the refractive indices and the angle of incidence, the second one is subject to the ability of the medium to scatter and absorb light, and therefore carries the spectral imprint of the composition and constitution of the medium. For this reason an adequate model of light propagation in the medium can be a tool for studying the spectral reflectance of surfaces in relation to the properties of the medium.

The more general approach to the propagation of light in a medium involves solving the radiative transfer equation (RTE) [8], but precisely its generality makes it a little used tool. A more practical approach for studying surface reflectance is to use bidirectional flux models, since the surface itself defines the geometry of both the system and the magnitude under analysis [9]. In addition, it is possible to demonstrate [10] that the results of a simple bidirectional model such as that of Kubelka–Munk converge to those of the RTE considering the simple assumptions of the theory, specifically bidirectional diffuse light flux, not considering polarization effects, homogeneous medium (in its first version), isotropic scattering, no specular reflection, and no effect of the lateral boundaries. In the case of particulate

✉ J. M. Saiz
saizvj@unican.es

[1] Group of Optics, Department of Applied Physics, Faculty of Science, University of Cantabria, Avda. de los Castros s/n, 39005 Santander, Cantabria, Spain

media, the absence of large particles and clusters is also assumed [11, 12].

Therefore, both a two-flux model and a four-flux model, if the conditions advise to include the mirror reflections, can be considered a good theoretical framework for addressing the surface spectroscopy problem. We will depend on this for our ability to adequately characterize the medium in terms of its absorption and scattering coefficients.

Of course, the media may have special characteristics, which in some cases have required adaptation of the most popular models. For example we can have a fluorescent medium [13], a medium sensitive to polarization, such as when there is some structural arrangement of the medium, a medium with particles of known sizes and concentration (Mie theory offers the possibility of "feeding" Kubelka–Munk theory with size-dependent values of the coefficients [14]), or, more importantly, the medium itself can present heterogeneities in the distribution of its properties, something that was first addressed by Kubelka himself in his paper of 1954 [15].

It is precisely the ability to easily adapt to these specificities of the environment that makes the Monte Carlo simulation methods—in which the medium and energy are discretized and the light–matter interaction translates into events with some probability—so attractive. The approach is similar to that of multilayer methods, widely used since Stokes used this formalism in 1860 [16], and both its validity and the convergence criteria have been duly established in recent works [17]. In addition to its capacity to deal naturally with issues such as heterogeneity [17] or fluorescence [18], the Monte Carlo solution offers the possibility of obtaining temporal resolution, allowing the calculation of transients, or the behavior of pulses without a large extra computational load.

In Sects. "Theoretical review" and "Numerical models" we will present, respectively, the theoretical framework of this work and the numerical models necessary to address it. In Sect. "Spectroscopy of diffuse media" we present some results related to spectral reflectance, to first describe the influence of scattering on color and then to comment on the influence of a lower substrate. Section "Spectroscopy of transmittance" will present findings related to transmission spectroscopy and Sect. "Time dependency" will show the potential of calculation methods to investigate the temporal dependence through some selected results. Finally, Sect. "Conclusions" presents a summary and the main conclusions of this work.

Theoretical review

The Kubelka–Munk (K–M) theory [2] is based on a simplified model of light propagation in a dull painted layer that is parallel to a plane support. Among many others,

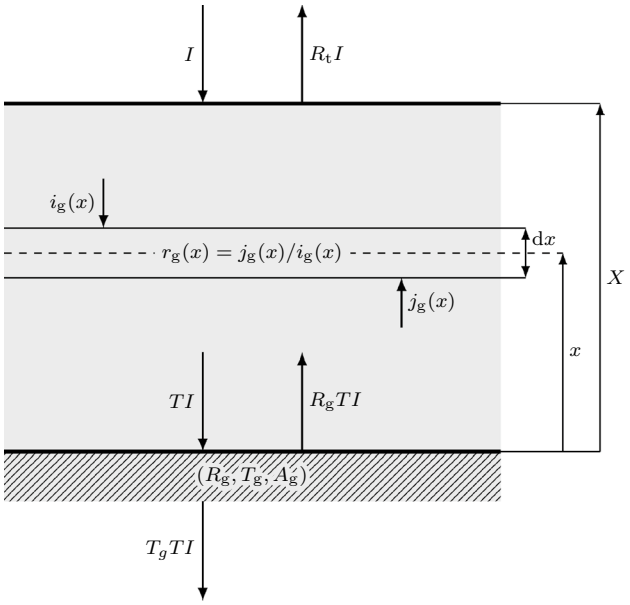

Fig. 1 Sketch of the light path of the Kubelka–Munk theoretical model showing a finitely thick plane-parallel light-scattering specimen (thickness ≡ X) placed in optical contact with an arbitrary substrate with known reflectance R_g, transmittance T_g, and absorptance $A_g = 1 - R_g - T_g$

the most important assumption involves perfectly diffused illumination of a perfectly dull material (see, e.g., [3, 9] and references therein). Figure 1 sketches the light path of the K–M theoretical model, using the same notation as the seminal work of Kubelka from 1948 [19]. A finitely thick plane-parallel light-scattering specimen (thickness ≡ X) is placed in optical contact with an arbitrary substrate with known reflectance R_g, transmittance T_g, and absorptance $A_g = 1 - R_g - T_g$. The specimen is illuminated from above (I being the intensity of illumination) and $i_g(x)$ and $j_g(x)$ are the intensities of the light traveling inside the specimen towards its unilluminated and its illuminated surface, with x being the distance from the specimen-substrate interface, as shown in Fig. 1. The subindex g always may indicate that the specimen is placed in optical contact with an arbitrary substrate with known reflectance R_g, transmittance T_g and absorptance $A_g = 1 - R_g - T_g$. R_t represents the total reflectance, i.e., the fraction of the incident light reflected by the specimen placed in optical contact with an arbitrary substrate. On the other hand, T denotes the fraction of the incident light transmitted by the specimen, that is, incident on the substrate. The total transmittance is thus given by $T_t = T_g T$.

Considering a specimen placed in optical contact with an arbitrary substrate with known reflectance R_g, transmittance T_g , and absorptance $A_g = 1 - R_g - T_g$, the fundamental equations of the K–M theory [2] are

$$-\mathrm{d}i(x) = -(S+K)i(x)\mathrm{d}x + Sj(x)\mathrm{d}x, \tag{1}$$

$$\mathrm{d}j(x) = -(S+K)j(x)\mathrm{d}x + Si(x)\mathrm{d}x, \tag{2}$$

where K and S are the absorption and backscattering coefficients, respectively, defined by the corresponding thickness of layer. After some basic math, the total reflectance, R_t, may be obtained:

$$R_t = \frac{\left(1 - aR_g\right)\sinh bSX + bR_g \cosh bSX}{\left(a - R_g\right)\sinh bSX + b\cosh bSX}, \tag{3}$$

where $a = 1 + K/S$ and $b = \sqrt{a^2 - 1}$. It may be shown that in the limit of infinite thickness, Eq. (3) reduces to the well-known K–M function R_∞

$$\lim_{X\to\infty} R_t \equiv R_\infty = a - b = 1 + \frac{K}{S} - \sqrt{\left(\frac{K}{S}\right)^2 + 2\left(\frac{K}{S}\right)}, \tag{4}$$

or

$$\frac{K}{S} = \frac{\left(1 - R_\infty\right)^2}{2R_\infty}. \tag{5}$$

The total intensity of light traveling inside the specimen at any given position x may be related to the transverse energy density $U(x)$

$$U(x) = I\frac{(a+1)\left(1 - R_g\right)\sinh bSx + b\left(1 + R_g\right)\cosh bSx}{\left(a - R_g\right)\sinh bSX + b\cosh bSX}. \tag{6}$$

The fraction of the incident light transmitted by the specimen, that is, incident on the substrate, is given by

$$T = \frac{b}{\left(a - R_g\right)\sinh bSX + b\cosh bSX} \tag{7}$$

which again reduces to Eq. (28) from Kubelka's paper [19] when $R_g = 0$. Making use of the transmittance of the substrate, T_g, the total transmittance is thus given by

$$T_t = T_g T = \frac{bT_g}{\left(a - R_g\right)\sinh bSX + b\cosh bSX} \tag{8}$$

Equations (3) and (8) allow us to calculate the total absorptance $A_t = 1 - R_t - T_t$ as well:

$$A_t = \frac{(a-1)\left(1 + R_g\right)\sinh bSX + b\left[\left(1 - R_g\right)\cosh bSX - T_g\right]}{\left(a - R_g\right)\sinh bSX + b\cosh bSX} \tag{9}$$

It may be shown that, thanks again to Eq. (7), Eq. (9) can be split into a contribution from the specimen alone, A, and another one coming from the substrate, so that

$$A_t = A + A_g T, \tag{10}$$

from where

$$A = \frac{(a-1)\left(1 + R_g\right)\sinh bSX + b\left(1 - R_g\right)(\cosh bSX - 1)}{\left(a - R_g\right)\sinh bSX + b\cosh bSX} \tag{11}$$

Surface corrections

The original K–M model does not take into account the reflections of light at the interface with air, which may be important. Saunderson [5] proposed a correction to take them into account. For his part, Murphy [20] extended the K–M model to the case of collimated illumination of optically rough surfaces, by modifying the Saunderson extension to allow treatment of reflection of collimated light from optically rough, optically smooth, and intermediate surfaces. Furthermore, Murphy introduced an expression for the reflection coefficient that allows the separation of reflectance into diffuse and collimated (specular) components, taking into account the characteristics of the integrating sphere used to measure the reflectance.

Other approaches

As previously mentioned, N-flux models allow us to solve the RTE in non-emitting plane-parallel media with infinite lateral extension, i.e., lateral scattering within the media is not taken into account and thus the equation depends only on one spatial direction. Indeed, they, the four-flux model in particular, can be derived from the scalar RTE. Although the vector RTE, which takes into account light polarization, has long been derived [21], currently there is no derivation of N-flux models from the vector RTE. Therefore, the largest source of error of these models arises from neglecting the fact that light can be polarized. In N-flux models light intensity is divided into N solid angles in the coordinate system.

We shall focus now in a particular case known as the four-flux model, where light propagation within the slab is modeled using two collimated and two diffuse fluxes, traveling towards its unilluminated and its illuminated surface. As light is scattered within the media, the total diffuse flux increases at the expense of collimated fluxes. De la Hoz and coworkers [22] provide the solution to the RTE using a four-flux model for this system when it is illuminated with partially collimated light, i.e., light that has both a collimated and a diffuse contribution. Expressions for the reflectance and transmittance in the aforementioned system are provided in [23] for the case of totally collimated incident light.

Taking into account the energy balances, the differential equations describing the system are[1]

$$\frac{dI_c}{dz} = -(\alpha + \beta)I_c, \tag{12}$$

$$\frac{dJ_c}{dz} = (\alpha + \beta)J_c, \tag{13}$$

$$\frac{dI_d}{dz} = \xi[(1-\sigma_d)\alpha(J_d - I_d) - \beta I_d] + \sigma_c \alpha I_c + (1-\sigma_c)\alpha J_c, \tag{14}$$

$$\frac{dJ_d}{dz} = \xi[\beta J_d + (1-\sigma_d)\alpha(J_d - I_d)] - \sigma_c \alpha J_c - (1-\sigma_c)\alpha I_c, \tag{15}$$

where α and β are the scattering and absorption coefficients per unit length, ξ is the average path length traveled by diffuse light as compared to collimated light, and σ_c and σ_d are the forward scattering ratio coefficients, i.e., the amount of light scattered into the forward hemisphere, for collimated and diffuse light respectively.

Explicit expressions for the effective light transfer across the system can be found in [22]. The system's total reflectance and transmittance have a specular contribution ($\mathcal{R}_c$, $\mathcal{T}_c$), the light that has remained collimated, and a diffuse contribution composed of the collimated incident light that is scattered ($\mathcal{R}_{cd}$, $\mathcal{T}_{cd}$) and the diffuse incident light ($\mathcal{R}_{dd}$, $\mathcal{T}_{dd}$). Therefore, the total reflectance and transmittance can be expressed as

$$\mathcal{R} = f\mathcal{R}_c + \mathcal{R}_d = f(\mathcal{R}_c + \mathcal{R}_{cd}) + (1-f)\mathcal{R}_{dd} \tag{16}$$

$$\mathcal{T} = f\mathcal{T}_c + \mathcal{T}_d = f(\mathcal{T}_c + \mathcal{T}_{cd}) + (1-f)\mathcal{T}_{dd}, \tag{17}$$

where f is the fraction of collimated incident light.[2]

As previously shown for the case of the two-flux model, a method to evaluate the contributions of the substrate to the total absorptance can also be derived. Indeed, the total absorptance of the system is simply the amount of light that is neither reflected nor transmitted. Mathematically is given by

$$\mathcal{A} = 1 - \mathcal{R} - \mathcal{T}. \tag{18}$$

Light can only be absorbed at either the film or the substrate. Thus, $\mathcal{A}$ can be rewritten as a sum of the light absorbed within the film $\mathcal{A}_f$ and within the substrate $\mathcal{A}_s$

$$\mathcal{A} = \mathcal{A}_f + \mathcal{A}_s = \mathcal{A}_f + f\mathcal{A}_{sc} + (1-f)\mathcal{A}_{sd}, \tag{19}$$

where A_{sc} and A_{sd} are the specular and diffuse contributions, respectively.

[1] Assuming z to be the distance from the illuminated surface (positive downwards).

[2] It is worth noting that the expressions from [23] are recovered if we illuminate the system with totally collimated light ($f = 1$).

Of course, the K–M model can be understood as a limiting case of the four-flux model in which the system is shined on with only perfectly diffuse light ($f = 0$), and only the film and the substrate are considered. Therefore, applying the conditions necessary to satisfy the assumptions made in the K–M model, we can recover the K–M expressions obtained in [17].

Spectrophotometry and colorimetry

From the spectral reflectance and transmittance, *XYZ* tristimulus values can be computed assuming a standard illuminant and a standard observer [24]. *XYZ* color coordinates can then be converted to $L^*a^*b^*$ color coordinates (L^* being the luminosity), which allow for the calculation of the chroma C^*, the hue $h°$, and the color difference ΔE.

$$\Delta E = \sqrt{\Delta L^{*2} + \Delta a^{*2} + \Delta b^{*2}}, \tag{20}$$

$$C^* = \sqrt{a^{*2} + b^{*2}}, \tag{21}$$

$$h° = \arctan\left(\frac{b^*}{a^*}\right), \tag{22}$$

Numerical models

Computing tools have proved very useful in solving problems by means of numerical simulations, and they are key in finding the behavior of light in dense or layered media [25]. Events like absorption or scattering can be implemented as events that may happen to each elemental light beam with a probability for each path unit. These models have proved themselves able to reproduce the analytical solutions given by theoretical models, as is the case of K–M's. This is why we are going to use a Monte Carlo simulation to accurately reproduce the analytical expressions we have found. In addition, numerical solutions will offer other results of interest for our system. Beyond the confirmation of the theory, it is interesting to notice that the agreement involves a mutual validation, so that the model can be looked upon as a tool with its own enlarged capabilities. Once convergence criteria have been found, the numerical model can be relied on as a distinct tool on which we can introduce a number of variations that depart notably from the assumptions that we required in the pursuit of analytical solutions.

In order to simulate the K–M theoretical model described in Sect. "Theoretical review", we implement a Monte Carlo approach. Specifically, we discretize the specimen into N layers and couple it to another layer representing the substrate. We assign an absorption and backscattering probability, PK and PS, respectively, to each layer (including

the substrate). PK and PS are the finite equivalents of the absorption and backscattering coefficients K and S, so that $PK \cdot N = KX$ and $PS \cdot N = SX$, or $PK \equiv K\mathrm{d}x$ and $PS \equiv S\mathrm{d}x$. We send N_T elemental light beams to the specimen and decide their fate according to algorithm 1.

simulation conditions. For its part, the total number of layers, N, which is given by

$$N = \frac{K+S}{PK+PS}X, \tag{23}$$

Algorithm 1 Monte Carlo approach algorithm.

$PK \leftarrow K\,\mathrm{d}x$ ▷ absorption probability
$PS \leftarrow S\,\mathrm{d}x$ ▷ backscattering probability

▷ Each incoming beam is initially moving to the right

while moving **do**
  $\rho \leftarrow$ uniformly distributed random number $\in (0, 1)$

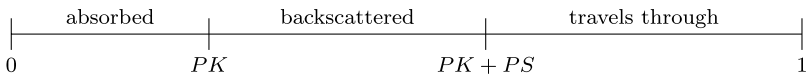

  if $\rho < PK$ **then**
    beam absorbed
    STOP
  else if $\rho < (PK + PS)$ **then** ▷ beam backscattered
    if moving to the right **then**
      if first layer **then**
        beam reflected
        STOP
      else
        reverse direction
        back one layer
    else
      reverse direction
      move one layer
  else ▷ beam travels through
    if moving to the right **then**
      if last layer **then**
        beam transmitted
        STOP
      else
        move one layer
    else
      if first layer **then**
        beam reflected
        STOP
      else
        back one layer

In its current state, the Monte Carlo simulation model outputs the total number of reflected, transmitted, and absorbed beams, the total number of beams hitting a given layer (related to the transverse energy density $U(x)$), and the total number of interlayer jumps of each beam before being either reflected, transmitted, or absorbed, which may be related to its time-of-flight (ToF). As it will be shown, the total number of incoming beams, N_T, determines the precision of the calculation, or the statistical uncertainty, i.e., the difference between consecutive realizations under the same

determines the accuracy of the calculation. The total event probability for each layer, $PK + PS$, directly determines the number of layers needed to correctly describe the physical phenomena taking place, and reproduce the theoretical results. In addition the obvious probability limit PK + PS $\leq$ 1is a criterion that must be established. As our Monte Carlo model implements the same assumptions as the K–M theory described in Sect. "Theoretical review", for a first verification we compare simulated and theoretical results of the total reflectance R_t. Figure 2 shows the difference (in percentage points) between simulated and

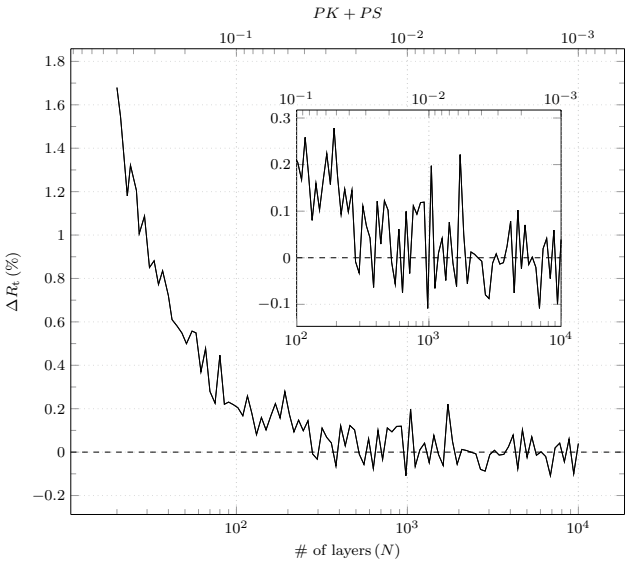

Fig. 2 Absolute difference (in percentage points) between simulated and theoretical results of the total reflectance ΔR_t, as a function of N (bottom axis) and PK + PS (top axis). $N_T = 100\,000$, $K/S = 9$, $SX = 1$. Transparent substrate. The inset shows a zoomed area between $N = 100$ and $N = 100\,000$

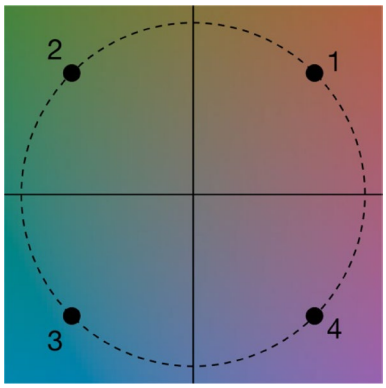

Fig. 3 Location of the four different dyes used in this study, all of them having the same chroma $C^* = 30$

theoretical results of the total reflectance ΔR_t as a function of the number of layers and $PK+PS$.

As can be seen in Fig. 2, for $PK + PS = 0.01$ the absolute difference between simulated and exact results is around 0.1 percentage points, so that we take

$$PK + PS \leq 0.01, \tag{24}$$

as a discretization criterion.

Spectroscopy of diffuse media

Scattering, thicknesses, and color

In this section we will use the K–M theory to study the color variation when depositing increasing thicknesses of different dyes on a given substrate, with special emphasis on the influence of the scattering coefficient S of the dyes, which characterizes the ability of a medium (dye in this case) to redirect a beam of light in directions other than that of incidence.

Figure 3 shows the location of the four different dyes, having all of them the same scattering properties, but different absorption properties (randomly selected to cover the color space, although all of them having the same chroma $C^* = 30$). These dyes have been deposited in a non-absorbing ($R_g + T_g = 1$) substrate, with reflectance $R_g = 0.1$.

In all figures, thin lines correspond to a constant scattering case, whereas thick lines correspond to a wavelength-dependent scattering case (assuming a Rayleigh-like—$S \propto 1/\lambda^4$—scattering dependance). Figure 4 shows the color coordinates L^*, C^*, and $h°$ in reflection, as a function of the thickness X. Figure 5 shows the color coordinates L^*, C^*, and $h°$ in transmission, as a function of the thickness X. Figure 6 shows the color difference (between constant S and wavelength-dependent S) as a function of the thickness X, both in reflection and transmission.

The smaller R_g is, the sooner it affects the spectral dependance of S the color in reflection. Colors with constant S all end up in a circle with saturation $C^* = 30$, by construction.

In transmission we always start from the same grayish color of the substrate (as R_g is constant) and we end up in black (also in the center of the $a^* - b^*$ plane). Saturation reaches a maximum, and luminosity ends in 0.

In reflection the color difference becomes more important sooner than in transmission.

Note that the scattering coefficient S is always linked to the thickness of the medium X, as the product SX. Its influence depends on how important this SX product is, compared to the absorption (KX). The reflectance of the substrate, R_g, has a greater influence on the color in transmission, while the spectral dependance of S has a greater influence on the color difference in reflection than in transmission.

Deviation from Beer–Lambert law

In this section we will analyze the transmittance variation when the scattering coefficient S of the media is increased. Figure 7 shows the total transmittance as a function of the thickness KX for two different values of K/S, with a constant value of K.

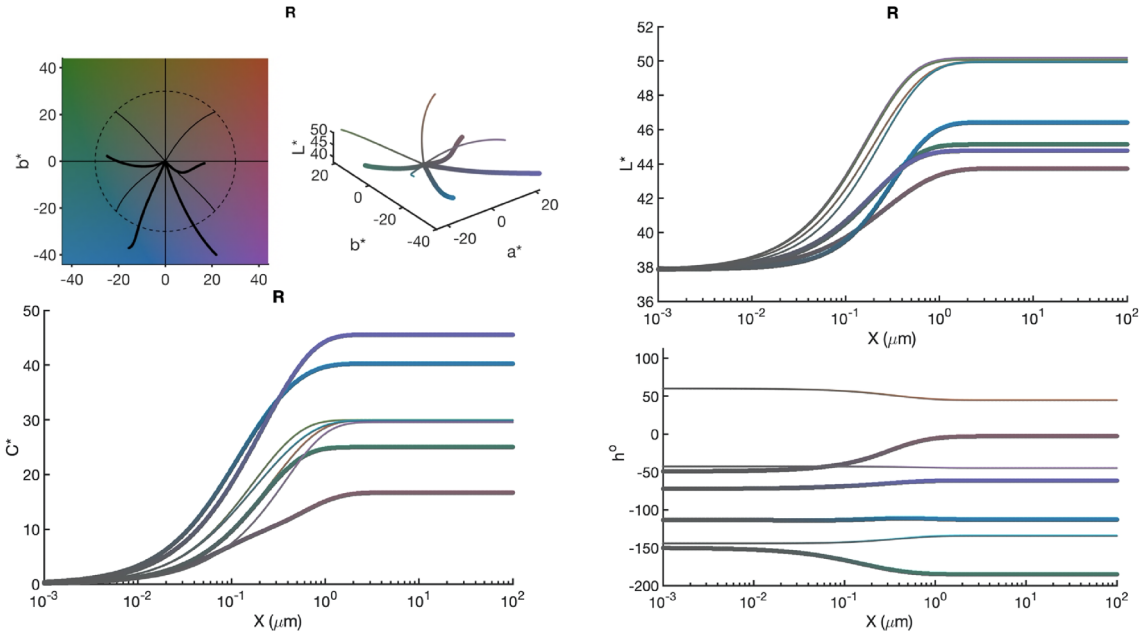

Fig. 4 Color coordinates L^*, C^* , and $h°$ in reflection, as a function of the thickness X

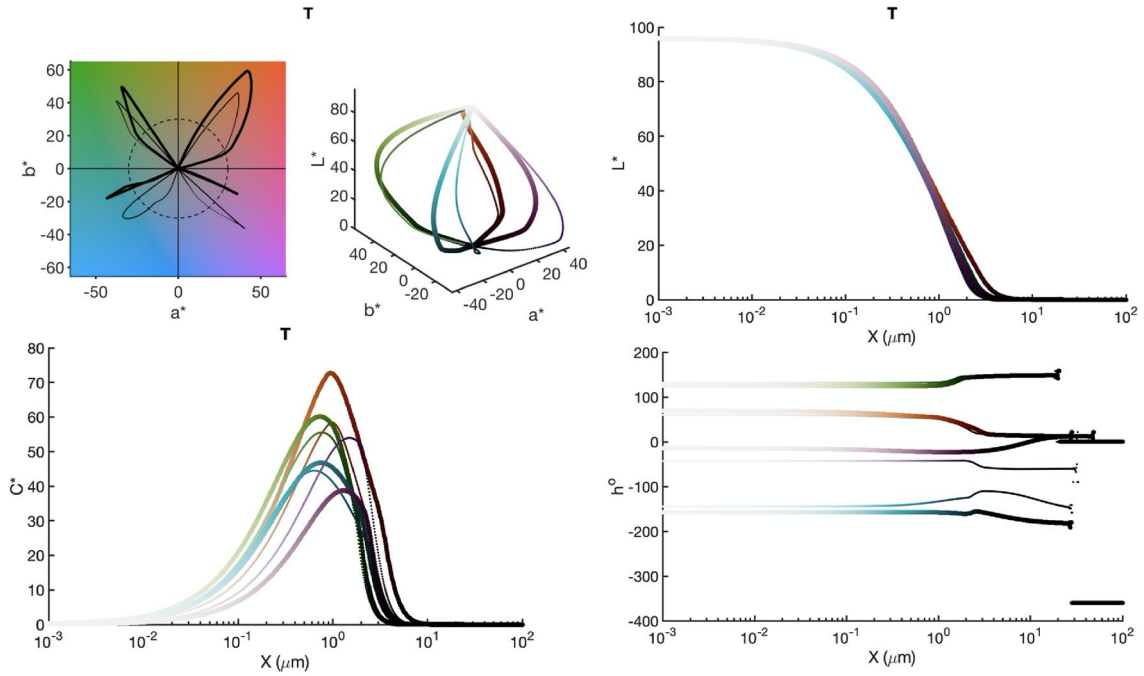

Fig. 5 Color coordinates L^*, C^* , and $h°$ in transmission, as a function of the thickness X

In the case of a highly absorbent media, $K/S = 100$ (blue line in Fig. 7), a decreasing curve is observed. In the semi-logarithmic scale it is almost a straight line, evidencing a behavior close to exponential. This is expected, since the transmission of a purely absorbent medium should show exponential behavior, given by the Beer–Lambert (B–L) law. This limiting case (pure absorption) can be obtained from Eq. (8) when $S \to 0$:

$$\lim_{S\to 0} T_t = T_g e^{-KX}. \tag{25}$$

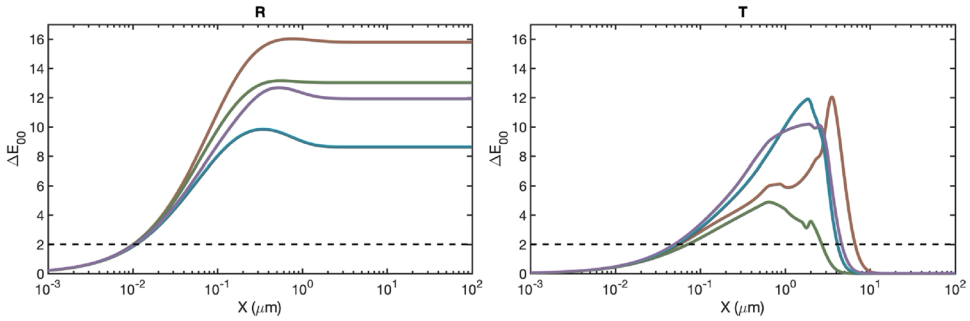

Fig. 6 Color difference ΔE_{00} (between constant S and wavelength-dependent S) as a function of the thickness X, both in reflection and transmission

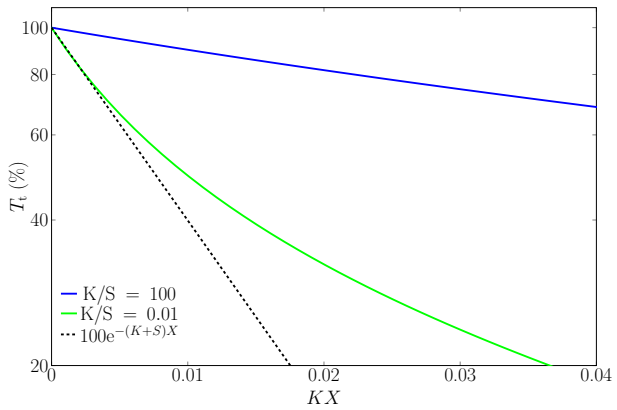

Fig. 7 The total transmittance T_t(solid lines), obtained from Eq. (8), as a function of KX (semi-logarithmic scale) for two values of K/S, simulating the case of pure absorbant media and a diffuse media. The case of absorption plus single scattering is also shown (dashed line), obtained from Eq. (26)

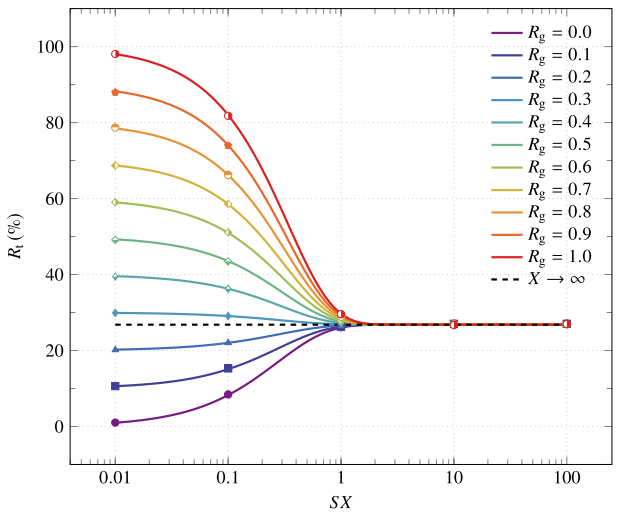

Fig. 8 Simulated (markers) and theoretical (solid lines) results of the total reflectance R_t for several values of R_g as a function of SX (logarithmic scale). Limit curves (dashed black lines) for the case of infinite thickness are also shown

When the K/S value decreases, i.e., S increases, the departure from an exponential becomes obvious ($K/S = 0.01$, green line in Fig. 7). A B–L exponential would require an extinction mechanism that is proportional to the intensity arriving at each point (like absorption), whereas scattering can reintroduce light into the original flux via multiple scattering. Single scattering, although unrealistic, is not a problem in terms of B–L law, as it contributes to extinction. If we only considered the absorption and the single scattering, we would obtain an ideal exponential in the form (dashed line in Fig. 7):

$$T_t = T_g e^{-(K+S)X}. \tag{26}$$

As it can be observed in Fig. 7 the transmittance in a medium with a strong scattering (green line) is higher than the ideal single-scattering one (dashed line). In such a dense medium light can be scattered many times, introducing scattered light into the transmittance flux, and this results in an increase of T. Interestingly, for small values of the thickness the curves overlap, showing that for very low thickness, for which the probability of multiple scattering events becomes negligible, the transmission reaches the exponential as a limiting case. Thus, when the specimen is either highly absorbent, Eq (25), or thin enough, Eq (26), a B–L law can be observed.

Substrate influence

In this section we will study the influence of the substrate on the total reflectance. Figure 8 shows theoretical results of the total reflectance of a specimen with $K/S = 1$, placed in optical contact with a substrate with varying reflectance R_g, as a function of SX. It can be seen that the influence of the substrate decreased as SX is increased. As expected, all results converge to the infinite thickness case (black dashed line) where the substrate color gets completely hidden by the specimen. Interestingly, there seems to be a special value of R_g for which $R_t = R_\infty$ regardless of the thickness of the specimen. It can be shown that this special value is actually $R_g = R_\infty = a - b$, obtained from Eq. (3) when $R_g \to R_\infty = a - b$.

Figure 8 also shows the simulated results of the total reflectance which fits with the theorical curve. For this case,

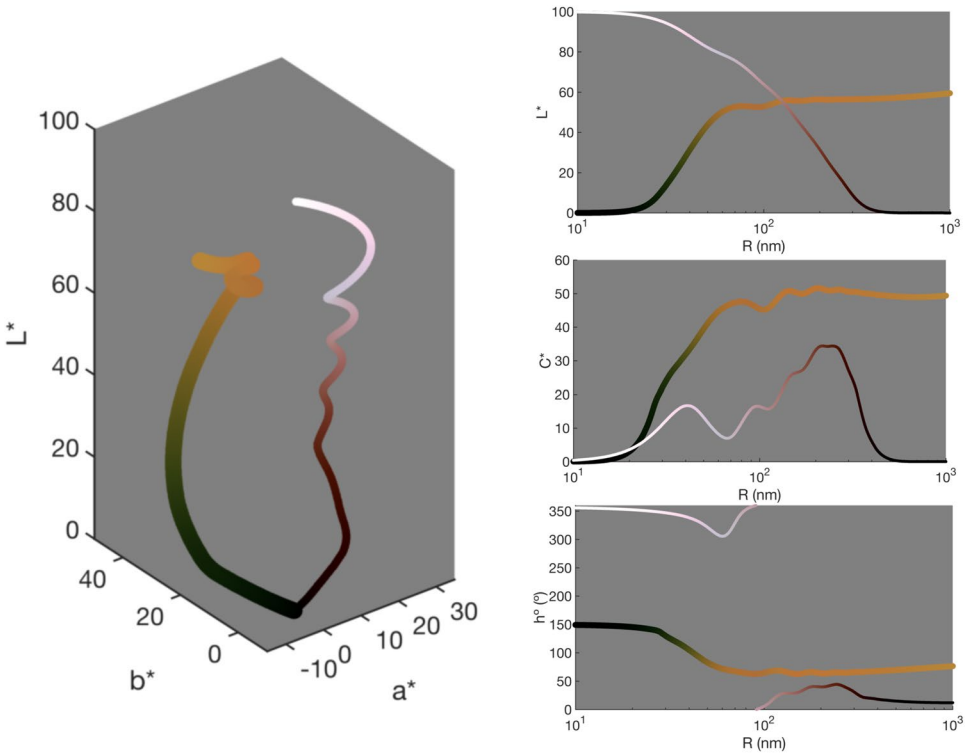

Fig. 9 Color trajectory (thick lines → reflection, thin ones → transmission) in the $L^*a^*b^*$ space and evolution of the luminosity L^*, chroma C^*, and hue $h°$ as the radius of the particles is varied from $R = 10\,\text{nm}$ to $R = 10^3\,\text{nm}$. The rest of the parameters are fixed: $n_{\text{sm}} = 1.33$ (water-embedding), $n = 10^6\,\text{mm}^{-3}$, and $h = 10\,\text{mm}$

the number of layers was $N = 20000$ in order to still meet Eq. (24) for the thickest specimen with $SX = 100$.

Spectroscopy of transmittance

In this section, we use the extended K–M theory to perform a colorimetric study of colloidal systems, connecting the particles' absorption and scattering cross sections as calculated with Mie theory with the absorption and scattering parameters associated with the K–M theory. The optical properties of the colloidal system are obtained by considering the actual size and composition of the particles, as well as the density. We consider a free-standing ($R_g = 0, T_g = 1$) gold colloid (Au, optical constants taken from Babar and Weaver [26]), of thickness h, embedded in a surrounding medium with refractive index n_{sm}. The parameters that we have varied are the radius of the particles R, the particle number density n, the thickness of the system h, and the refractive index of the surrounding medium n_{sm}. According to the model, the system is solved as a multilayer of arbitrarily thin layers, with no lateral boundaries.

In the case of a colloidal medium, the origin of the scattering and absorption is microscopically located in the particles that have some absorption and scattering cross sections, C_{abs} and C_{sca}.

From Mie theory [27]

$$C_{\text{sca}} = \frac{2\pi}{k^2}\sum_{n=1}^{\infty}(2n+1)\left(|a_n|^2 + |b_n|^2\right), \tag{27}$$

$$C_{\text{abs}} = C_{\text{ext}} - C_{\text{sca}}, \tag{28}$$

where a_n and b_n are the electric and magnetic Mie coefficients, respectively, and

$$C_{\text{ext}} = \frac{2\pi}{k^2}\sum_{n=1}^{\infty}(2n+1)\Re\{a_n + b_n\}, \tag{29}$$

with $k = 2\pi n_{\text{sm}}/\lambda$. The K–M absorption and scattering coefficients are then given by [28]

$$K = 2 \times C_{\text{abs}} \times n \tag{30}$$

$$S = \frac{3}{4} \times C_{\text{sca}} \times \left(1 - g_{\text{sca}}\right) \times n, \tag{31}$$

where n is the particle number density and g_{sca} is the asymmetry parameter.[3] In the context of effective medium theories, a filling fraction f is usually defined, as $f = nv$, where v is the volume of an individual particle.

Trajectories in the color space are calculated from both reflection and transmission spectra, studying the influence

[3] Calculated in terms of the Mie coefficients as well, see, e.g., [27, p. 120].

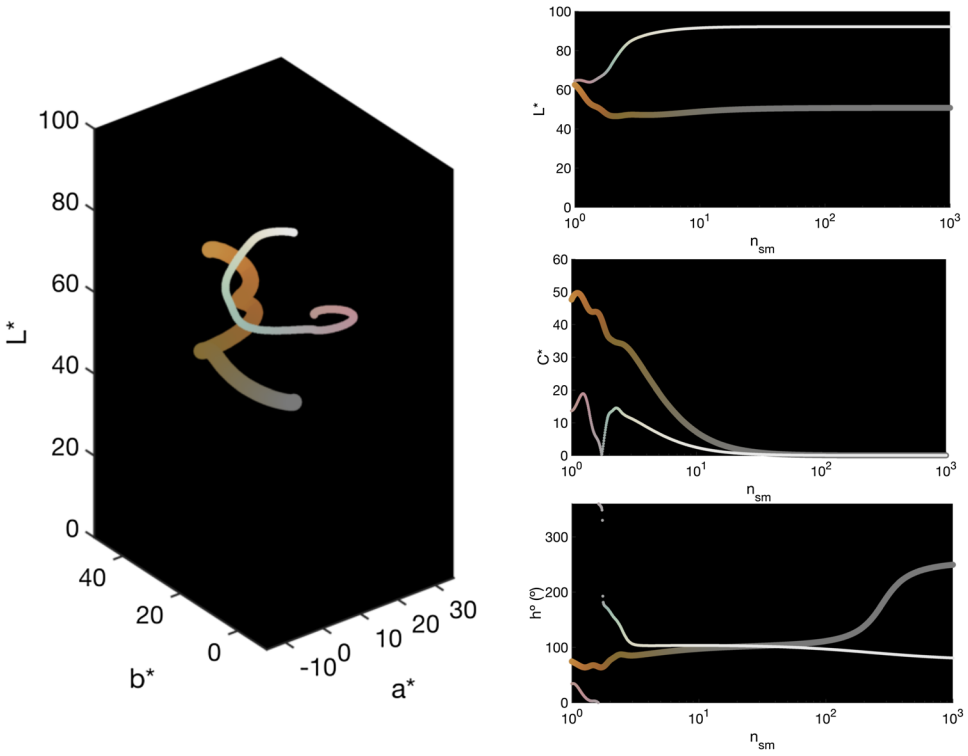

Fig. 10 Color trajectory (thick lines → reflection, thin ones → transmission) in the $L^*a^*b^*$ space and evolution of the luminosity L^*, chroma C^*, and hue $h°$ as the (real) refractive index of the surrounding medium is varied from $n_{sm} = 1$ to $n_{sm} = 1000$. The rest of the parameters are fixed: $R = 100\,\text{nm}$, $n = 10^6\,\text{mm}^{-3}$, and $h = 10\,\text{mm}$

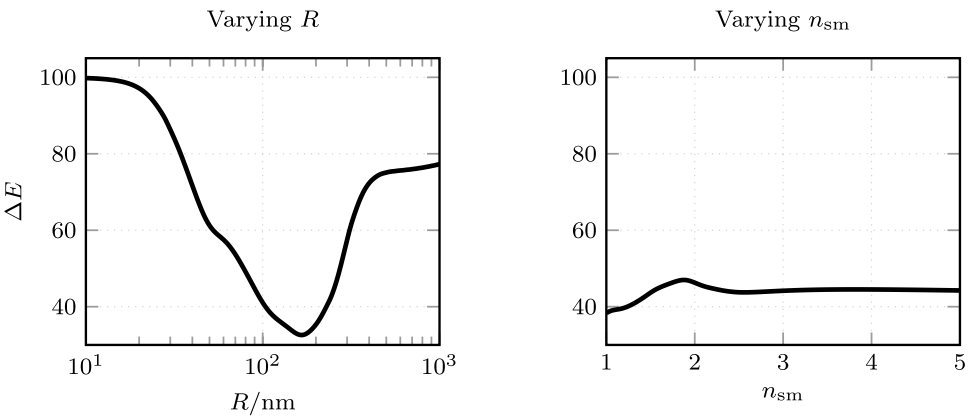

Fig. 11 Color difference ΔE between reflection and transmission as a function of the particle radius R and the refractive index of the surrounding medium n_{sm}

of two parameters: the radius of the nanoparticle and the refractive index of the surrounding medium.

Varying the radius of the particles

Figure 9 shows the color trajectory in the $L^*a^*b^*$ space and the evolution of the luminosity L^*, the chroma C^*, and the hue $h°$ as we vary the radius of the particles, R. The rest of the parameters are fixed: $n_{sm} = 1.33$ (water-embedding), $n = 10^6\,\text{mm}^{-3}$, and $h = 10\,\text{mm}$. The maximum filling fraction achieved is $f = 0.0042$.

As can be seen in Fig. 9, we start from black in reflection and white (as D65 represents white light) in transmission, i.e., for very small particles ($R = 10\,\text{nm}$), all light is transmitted through the system. The opposite happens for very large particles ($R = 1\,\mu\text{m}$), where all light is reflected, reaching an orangish color in reflection and perfect black in transmission (no transmitted light at all). In reflection, we observe greenish and orangish colors as we increase the radius of the particles, whereas more pinkish and reddish colors are observed in transmission.

Varying the refractive index of the surrounding medium

Figure 10 shows the color trajectory in the $L^*a^*b^*$ space and the evolution of the luminosity L^*, the chroma C^*, and the hue $h°$ as we vary the refractive index of the surrounding medium, n_{sm} (considered dielectric). The rest

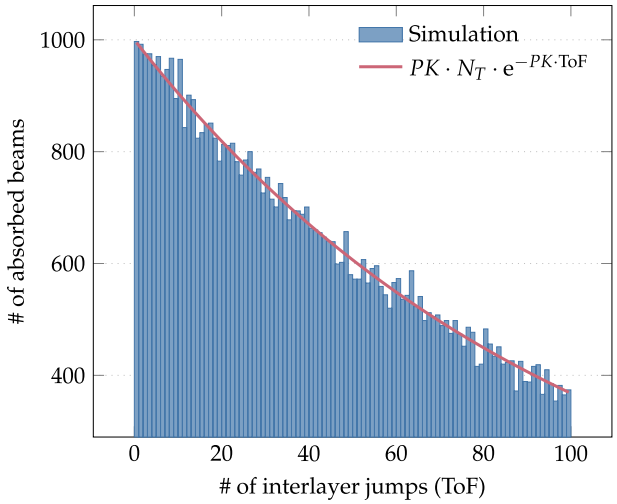

Fig. 12 Histogram of the number of interlayer jumps (ToF) of the absorbed beams where we have sent $N_T = 10^5$ beams to a system with $KX = 1$ and $S = 0$ discretized with $N = 10^2$ layers, placed on top of a perfectly transparent substrate $(R_g, T_g, A_g) = (0, 1, 0)$

of the parameters are fixed: $R = 100\,\text{nm}$, $n = 10^6\,\text{mm}^{-3}$, and $h = 10\,\text{mm}$. The filling fraction is again constant, $f = 4.19 \times 10^{-6}$.

As can be seen in Fig. 10, when varying the refractive index of the surrounding medium, we start from our well-known orangish and pinkish colors, in reflection and transmission, respectively, corresponding to spherical particles of radius $R = 100\,\text{nm}$ with a particle number density $n = 10^6\,\text{mm}^{-3}$ and a thickness $h = 10\,\text{mm}$. As the refractive index of the surrounding medium is increased, color in reflection loses chroma, slightly increasing its hue (turning yellowish) until all color is lost, ending in a medium gray ($L^* \approx 50$). In transmission, however, we go from pink to almost white, passing through light green and yellow, which implies a dramatic variation in hue.

Color difference between reflection and transmission

Figure 11 shows the color difference ΔE between reflection and transmission as we vary the particle radius R and the refractive index of the surrounding medium n_{sm}.

When varying either the radius of the particles, the particle number density, or the thickness of the system, we always start from the maximum color difference ($\Delta E = 100$), as we are comparing black (reflection) and white (transmission). A similar result is obtained at the other end (ΔE around 80), where we are comparing orange (reflection) and black (transmission).

Table 1 System properties

i	n	$\alpha\,(\text{mm}^{-1})$	$\beta\,(\text{mm}^{-1})$	$h\,(\text{mm})$	l
1	1.5	0.1	0.1	1	502
2	1.8	1	1	1	502
3	1.5	0	0	2	1004

Physical properties of the two coatings ($i = 1, 2$), and the substrate ($i = 3$) of the system under study. n is the refractive index, α (β) is the scattering (absorption) coefficient per unit length, h is the width of the layer, and l is the number of layers into which the corresponding medium has been discretized

The minimum color difference ($\Delta E \approx 40$, still huge[4]) is found for values $R \approx 100\,\text{nm}$, $n \approx 10^6\,\text{mm}^{-3}$, and $h \approx 10\,\text{mm}$. These are the values that have been used for studying the evolution of the color when the refractive index of the surrounding medium is increased. Figure 11 shows that the color difference between reflection and transmission is reasonably constant as n_{sm} is increased, reaching its maximum value ($\Delta E = 46.99$) for $n_{sm} = 1.876$.

Time dependency

As a result of the way in which a Monte Carlo model handles the propagation of light in the form of elemental beams that make their progress through the system in discrete steps, it is possible to analyze the output not just as a purely cumulative mechanism to construct the reflectance or transmittance factors but also in terms of their history.

A very simple example of this is shown in Fig. 12, where the histogram of the number of interlayer jumps (proportional to the time of flight, ToF), is represented for an almost transparent medium, with $KX = 1$ and $S = 0$ (small absorption and no scattering). The substrate is chosen here as totally transparent $(R_g, T_g, A_g) = (0, 1, 0)$ and the discretization is $N = 10^2$ layers and $N_T = 10^5$ elemental beams. In these conditions the system works in an extremely simple single-flux fashion. The result is an exponentially decreasing curve that can be easily fitted with the parameters of the problem (red line). For the proposed conditions the number of jumps before being absorbed is proportional to the penetration depth, so that this histogram is just a representation of the B–L law, Eq. (25).

This Monte Carlo simulation could be helpful, by changing the desired parameters, to understand the origins of the deviations from B–L law, a classical problem that keeps attracting the interest of researchers in chemistry and physical optics [29].

[4] In this case we are comparing orange and pink, which are two perfectly distinguishable colors.

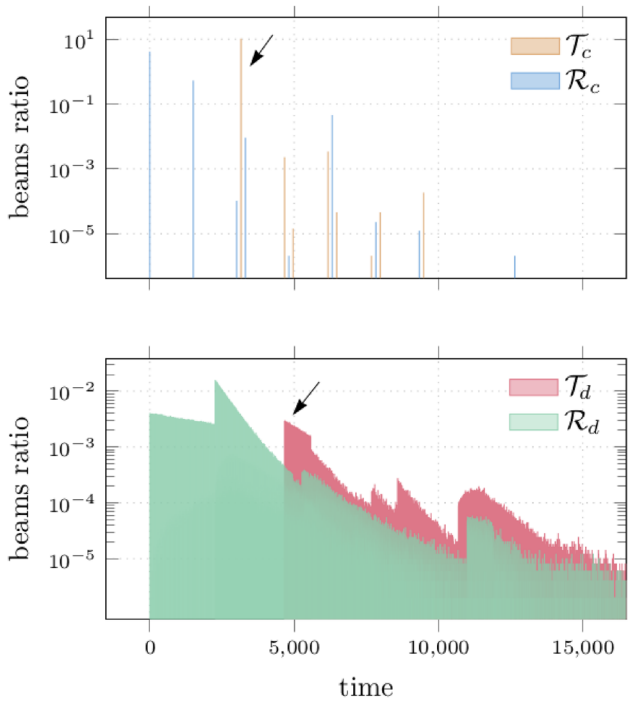

Fig. 13 Response function of the system to a delta-like pulse. Histogram showing the ratio of collimated and diffuse beams that have been either reflected or transmitted as a function of time. The bin width is equal to a time element Δt. The total number of incident beams utilized in this simulation is $N_T = 5 \times 10^7$. The arrows show two important peaks that are discussed in the text

Another less simple example of the ability of Monte Carlo simulations to deal with time variations is the propagation of pulses through stratified translucent media. Let us consider an ultrashort collimated pulse (modelled as a $\delta(t = 0)$ function with N_T elemental beams) and a system consisting of two coatings applied to a transparent substrate.

The properties of the three regions are shown in Table 1, the second layer being a denser one with higher values of scattering and absorption. The system is discretized into $N = 2008$ layers, satisfying convergence criteria, and $N_T = 5 \times 10^7$, enough to get stable results. The basic time unit Δt corresponds to the collimated beam crossing a layer of index $n = 1$. For other indices the time increases accordingly ($n\Delta t$ for a collimated elemental beam, $\xi n\Delta t$ for a diffuse one, ξ being the increase of path due to the obliquity of diffuse light).The part of the beam that remains collimated (ballistic light) produces sharp peaks at fixed times in both reflectance and transmittance, while the diffuse magnitudes appear spread over time.

In Fig. 13 the reflectance and transmittance of the system are represented separately for the collimated and diffuse output beams. These histograms represent the impulse–response of the system. For any other pulse with a time dependence $f(t)$ these impulse–response distributions should be convoluted with $f(t)$ in order to obtain the actual collimated and diffuse outputs. The addition of both would produce the overall transmittance and reflectance. For the case of the ultrashort pulse represented by the function $\delta(t = 0)$, both the reflectance and transmittance contain a sequence of peaks—coming from the reflections produced at different boundaries—plus a background light corresponding to the scattered light. In the reflectance signal just four peaks could stand out clearly (SNR > 2) from the noisy background, none of them later than $t = 7 \times 10^3 \Delta t$, after which the diffuse tail is dominant. For transmission, the peak at $t = 3163\Delta t$ (direct collimated transmission: $t = (n_1 l_1 + n_2 l_2 + n_{sl_s})\Delta t$) is the dominant one (see arrow in Fig. 13). Another peak, slightly later than $t = 6 \times 10^3 \Delta t$, would be the last one to stand out clearly over the background light (see other arrow).

An interesting aspect that is worth explaining is the time delay between the first collimated and diffuse transmitted beams ($t = 3163\Delta t$ for the collimated and $t = 4670\Delta t$ for the diffuse). This is really an artifact of the model: all the diffuse beams are supposed to travel in the same oblique trajectory: the one that doubles the path ($\xi = 2$) of the collimated beams. This value is correct as an average, but we take it for every beam for the sake of simplicity. Selecting ξ for each scattering event would soften the sharp variations in the diffuse distribution and match the resulting tails with their corresponding collimated beams.

For instance, the origin of the sharp edge observed in $t = 10693\Delta t$ is closely related to the specular transmission peak at $t = 6175\Delta t$. This specular peak represents transmission with only one internal reflection taking place in the third layer (substrate). Under this transmission mechanism, when forward scattering appears, it has to occur while passing through the first and second coatings, because there is no scattering in the third one (the substrate is transparent). In other words, scattering can occur as early as the first contact with the specimen and as late as the last contact with the second coating, producing total transient times in the interval $t = (10693, 12350)\Delta t$. All remarkable features in these plots can be explained in similar terms.

Finally, it is worth commenting that other events can be time-resolved by this description, like the transient states before reaching stationary solutions for $R(t)$ and $T(t)$, or the case of fluorescence and phosphorescence equilibria [18], where some additional probabilities have to be introduced to account for both the "charging" process (specific absorption and transfer to metastable states) and the emission in longer wavelengths.

Conclusions

In this article we have reviewed the fundamentals of the Kubelka–Munk theory, a very interesting framework for solving the problem of the propagation of light in an

absorbent/scattering medium. We have presented it in an extended version that includes the existence of a substrate underneath, showing its main analytical results, conditions of validity, and the main variations that allow you to implement the problem of boundaries in a realistic way. Both the original two-flux and the more modern four-flux formalisms have been included in the study. The importance of these solutions has been underlined by their application to the calculation of spectral transmittance and reflectance curves. This has been shown for several examples, like analyzing the impact of the scattering coefficient and the thickness on the spectral reflectance of diffuse media, or the effect of the scattering properties of suspended particles on the spectral transmittance of colloids. An interesting addition to these results is the color analysis, or the possibility of summarizing the evolution of the spectral response with just a few parameters, easily interpreted by our perception (color difference is often mentioned as a tool for the diagnosis of many processes) and very often it is directly accessible for our instruments. Another aspect that has been examined is the numerical resolution of this problem, which is very important since the analytical solution is available only under very specific conditions. When the medium is not homogeneous, the diffusing element is not isotropic, or if complex light–matter interactions appear (inelastic scattering, photoluminescence, non-linear phenomena), it may happen that we need numerical solutions of the equations or even that we need to rethink new balance equations. For all these situations, the Monte Carlo approach has proved to be ideal. Once you have an adequate discretization of the medium and light, the passage of time is discretized and the interaction translates into probabilities of events for each interval. This way of proceeding not only allows a cumulative record of magnitudes like the spectral reflectance but also a temporary solution that allows one to resolve transient states, pulses, etc., giving an added value to this method. As an example of this we have shown the time histogram of "photons" in a purely absorbent medium, showing the expected fit to a Beer–Lambert law.

Acknowledgements This research has been supported by the Spanish Ministry of Science and Innovation (MICINN) under project PGC2018-096649-B-I00.

References

1. Schuster A (1905) Radiation through a foggy atmosphere. Astrophys J 21:1
2. Kubelka P, Munk F (1931) An article on optics of paint layers. Z Tech Phys 12:593–609
3. Dzimbeg-Malcic V, Barbaric-Mikocevic Z, Itric K (2011) Kubelka-Munk theory in describing optical properties of paper (I). Tech Gaz 18(1):117–124
4. Dzimbeg-Malcic V, Barbaric-Mikocevic Z, Itric K (2012) Kubelka-Munk theory in describing optical properties of paper (II). Tech Gaz 19(1):191–196
5. Saunderson JL (1942) Calculation of the color of pigmented plastics. J Opt Soc Am 32(12):727–736
6. Atherton E (1955) The relation of the reflectance of dyed fabrics to dye concentration and the instrumental approach to colour matching. J Soc Dyers Colour 71(7):389–398
7. Hui Y (1992) Encyclopedia of food science and technology, encyclopedia of food science and technology, vol 1. Wiley, New York
8. Chandrasekhar S (2013) Radiative transfer. Courier corporation. Dover Publications, New York
9. Philips-Invernizzi B, Dupont D, Cazé C (2001) Bibliographical review for reflectance of diffusing media. Opt Eng 40(6):1082–1092
10. Pierce PE, Marcus RT (1997) Radiative transfer theory solid color-matching calculations. Color Res Appl 22:72–87. https://doi.org/10.1002/(SICI)1520-6378(199704)22:2<72::AID-COL3>3.0.CO;2-0
11. Kumar A, Choudhury A (2015) Principles of colour and appearance measurement, vol 2. Visual measurement of colour, colour comparison and management. Woodhead Publishing, Elsevier Science. eBook ISBN: 9781782423881
12. Vargas WE, Niklasson GA (1997) Applicability conditions of the Kubelka-Munk theory. Appl Opt 36(22):5580–5586
13. Fukshansky L, Kazarinova N (1980) Extension of the Kubelka-Munk theory of light propagation in intensely scattering materials to fluorescent media. J Opt Soc Am 70(9):1101–1111
14. Mills D, Subbaswamy K (1981) II Surface and size effects on the light scattering spectra of solids, vol 19. Elsevier, Amsterdam, pp 45–137. https://doi.org/10.1016/S0079-6638(08)70201-4
15. Kubelka P (1954) New contributions to the optics of intensely light-scattering materials. Part II: nonhomogeneous layers. J Opt Soc Am 44(4):330–335
16. Stokes GG (1860) On the intensity of the light reflected from or transmitted through a pile of plates. R Soc Lond 11:545–557
17. Alcaraz de la Osa R, García Alonso A, Ortiz D, González F, Moreno F, Saiz JM (2016) Extension of the Kubelka-Munk theory to an arbitrary substrate: a Monte Carlo approach. J Opt Soc Am A 33(10):2053. https://doi.org/10.1364/josaa.33.002053
18. Pérez M, González I, Saiz J, Moreno F, González F (2009) Saturation processes of photoluminescent pigments embedded in sinterized glass. J Modern Opt 56(13):1466–1474. https://doi.org/10.1080/09500340902990015
19. Kubelka P (1948) New contributions to the optics of intensely light-scattering materials. Part I. J Opt Soc Am 38(5):448–457
20. Murphy AB (2006) Modified Kubelka-Munk model for calculation of the reflectance of coatings with optically-rough surfaces. J Phys D Appl Phys 39(16):3571–3581
21. Mishchenko MI (2002) Vector radiative transfer equation for arbitrarily shaped and arbitrarily oriented particles: a microphysical derivation from statistical electromagnetics. Appl Opt 41(33):7114–7134
22. de la Hoz E, Alcaraz de la Osa R, Ortiz D, Saiz JM, Moreno F, González F (2019) Physically meaningful Monte Carlo approach to the four-flux solution of a dense multilayered system. J Opt Soc Am A 36(2):292. https://doi.org/10.1364/josaa.36.000292
23. Vargas WE, Niklasson GA (1997) Pigment mass density and refractive index determination from optical measurements. J Phys Condens Matter 9(7):1661–1670
24. Wyszecki G, Stiles WS (1982) Color Science: concepts and methods, quantitative data and formulae, 2nd edn. Wiley, New York
25. Coppel LG, Edström P, Lindquister M (2009) Open source Monte Carlo simulation platform for particle level simulation of light scattering from generated paper structures. PRS 2009. Kuopio, Finland, pp 1–10

26. Babar S, Weaver JH (2015) Optical constants of Cu, Ag, and Au revisited. Appl Opt 54(3):477–481
27. Bohren CF, Huffman DR (1983) Absorption and scattering of light by small particles. Wiley, New York
28. Kerker M, Scheiner P, Cooke DD, Kratohvil JP (1979) Absorption index and color of colloidal hematite. J Colloid Interface Sci 71(1):176–187
29. Mayerhöfer TG, Höfer S, Popp J (2019) Deviations from Beer's law on the microscale—nonadditivity of absorption cross sections. Phys Chem Chem Phys 21(19):9793–9801. https://doi.org/10.1039/c9cp01987a